crystals

MDPI

Article

Conformation-Dependent Electron Donation of *Nido*-Carborane Substituents and Its Influence on Phosphorescence of Tris(2,2′-bipyridyl)ruthenium(II) Complex

Kyoya Uemura, Kazuo Tanaka * and Yoshiki Chujo

Department of Polymer Chemistry, Graduate School of Engineering, Kyoto University Katsura, Kyoto 615-8510, Japan; i30s1992@i.kyoto-u.ac.jp (K.U.); chujo@poly.synchem.kyoto-u.ac.jp (Y.C.)
* Correspondence: tanaka@poly.synchem.kyoto-u.ac.jp; Tel.: +81-75-383-2604; Fax: +81-75-383-2605

Abstract: In this work, we report the synthesis of the *nido*-carborane-substituted ruthenium complexes and the substituent effects of *nido*-carboranes on the optical properties. Initially, from the optical measurements, it is shown that deep-red phosphorescence was obtained from the synthesized molecule, and the phosphorescent quantum yields were significantly improved by loading onto a polyethylene glycol film. This result represents that *nido*-carborane can work as a strong electron donor and should be an effective unit for enhancing the solid-state phosphorescence of ruthenium complexes. Further, it is suggested that the electron-donating properties of the *nido*-carborane units and subsequently the optical properties can be tuned by controlling the conformation of the *nido*-carborane units with the steric substituents. We demonstrate in this study the potential of *nido*-carborane as a building block for constructing optical materials as well as fundamental information regarding electronic interactions with π-conjugated systems.

Keywords: carborane; ruthenium; phosphorescence; deep-red luminescence

Citation: Uemura, K.; Tanaka, K.; Chujo, Y. Conformation-Dependent Electron Donation of *Nido*-Carborane Substituents and Its Influence on Phosphorescence of Tris(2,2′-bipyridyl)ruthenium(II) Complex. *Crystals* **2022**, *12*, 688. https://doi.org/10.3390/cryst12050688

Academic Editor: Simon Duttwyler

Received: 20 April 2022
Accepted: 9 May 2022
Published: 11 May 2022

1. Introduction

Tris(2,2′-bipyridyl)ruthenium(II) complex ($[Ru(bpy)_3]^{2+}$) is recognized as one of many versatile transition metal complexes because of their unique properties, such as high chemical stability, visible light photoredox property [1,2], metal-to-ligand charge transfer (MLCT) [1,3], long-lived T_1 excited state [3], and room-temperature phosphorescence [4,5]. So far, $[Ru(bpy)_3]^{2+}$ and its derivatives have been utilized as a platform for the development of photochemistry, photophysics, electrochemistry, photocatalysis, and chemiluminescence. Particularly, the red phosphorescence of these complexes has attracted a great deal of attention for the numerous applications in organic light-emitting diodes [6,7], oxygen chemosensors, and bio-imaging [8]. Considerable efforts have been devoted to the synthesis of high-performance complexes with longer wavelengths and higher phosphorescent efficiency through the proper choice of the coordinated ligands. The one effective strategy to induce redshift into the emission band of $[Ru(bpy)_3]^{2+}$ is the introduction of strong electron-donating groups to the 4,4′-positions in the bipyridine ligand. For example, a series of ruthenium complexes containing hydroxyl-substituted polypyridyl ligands were studied by Jared and co-workers, and a significant redshift in the absorption and emission spectra was observed, originating from the ligand's orbitals heavily mixed with the d-orbitals of ruthenium [9]. However, these deep-red phosphorescent complexes exhibit poor emission, especially in the solid-state, due to triplet–triplet annihilation, low band gap, and concentration quenching. Therefore, the development of deep-red phosphorescent materials with high emission efficiencies is still challenging and required for further applications.

7,8-Dicarba-*nido*-undecaborate anion (*nido*-carborane) is the class of polyhedral boron–carbon molecular clusters (Figure 1). *nido*-Carborane is usually synthesized from *o*-carborane,

which is the icosahedral boron–carbon cluster, by deboronation. Both carboranes have high stabilities and rigid structures because the skeleton electrons are delocalized three-dimensionally through their three-center–two-electron (3c, 2e) bonds [10,11]. Moreover, characteristic electronic properties have been discovered. Electron-withdrawing properties of *closo*-carboranes have been reported in various carborane-related compounds [12–14], meanwhile, the electronic structures of *nido*-carboranes give unique electron-donating properties as substituents or ligands [15,16]. From these notable properties, *nido*-carborane derivatives have been studied in a variety of areas, for example, boron neutron capture therapy (BNCT) [17], coordination chemistry [18–25], and catalysts [26].

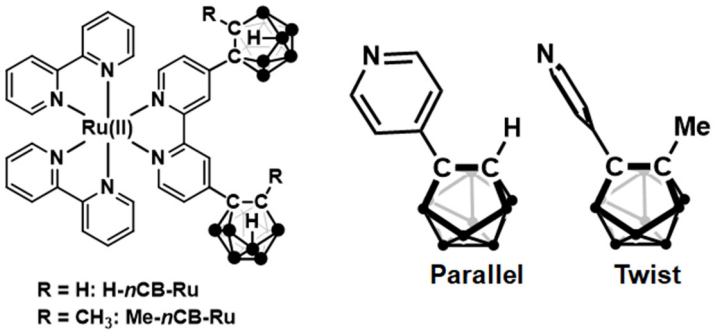

Figure 1. Chemical structures and molecular conformations of the ruthenium complexes used in this study.

Because of such unique electronic structures, we focus on carboranes as an element-block, which is a minimum functional unit containing heteroatoms, for developing opto-electronic materials [27–30]. It is established that *o*-carborane works as a strong electron acceptor when bonded to aromatic units at the carbon, and especially its electron-accepting ability is significantly dependent on the angle between the π-plane and the direction of the C–C bond in *o*-carborane [31–38]. Therefore, highly-efficient luminescent materials with variable colors have been developed by blocking intramolecular motions at the *o*-carborane unit [39–41]. Furthermore, luminochromic behaviors were also observed based on solid-state luminescent *o*-carboranes [42–50]. In contrast, it is known that *nido*-carboranes can work as strong electron donors [15,16]. In recent years, emissive materials concerning *nido*-carborane were also studied. For example, we have reported that stimuli-responsive solid-state luminochromism was observed from the helicene-tethered *nido*-carborane [51]. Therefore, *nido*-carborane is expected as a potential element block for obtaining further functional materials.

In this study, we synthesized *nido*-carborane-substituted ruthenium complexes, **Me-*n*CB-Ru** and **H-*n*CB-Ru**, with or without the methyl group at the carbon in the *nido*-carborane unit and performed optical measurements in various media (Figure 1). The synthesized complexes showed deep-red phosphorescence, and we obtained higher emission efficiencies in the polyethylene glycol (PEG) film by suppressing molecular motions. This result means that *nido*-carborane should work as a strong electron donor. Moreover, we performed detailed studies on the substituent effect on phosphorescent properties and theoretical data. Accordingly, it was revealed that the methyl substituent plays a critical role in molecular conformation because of steric hindrance, and the electron-donating properties of the *nido*-carborane units should be enhanced and weakened at the parallel and twisted conformation, respectively. As a result, optical properties were varied by changing the degree of electronic interaction between the ruthenium complex moiety and the *nido*-carborane units. This is the first study, to the best of our knowledge, not only to present phosphorescent films containing *nido*-carborane but also to show the conformation-dependent electronic interaction of *nido*-carborane to π-conjugation and followed by optical properties.

2. Results and Discussion

2.1. Synthesis of Ru(II) Complexes

Although it is implied that the substituent on the *nido*-carborane unit might be responsible for the molecular conformation followed by electronic interaction with π-conjugated units, the detail mechanism is still unclear. Particularly, in comparison to the tunability of the electron-accepting ability of *o*-carborane by modulating the angle toward the π-plane, the relationship between molecular conformation and electron-donating ability of the *nido*-carborane unit is still veiled. Furthermore, there are only a few examples to offer *nido*-carborane-based phosphorescent materials. Therefore, we synthesized *nido*-carborane-substituted ruthenium complexes with variable substituents at the carbon in the *nido*-carborane unit to comprehend the relationship between molecular conformation and electronic properties.

Two ruthenium complexes, **H-*n*CB-Ru** and **Me-*n*CB-Ru** were synthesized (Scheme 1). The *nido*-carborane-substituted bipyridine ligand **L1** was synthesized by the modified procedure including Migita–Kosugi–Stille coupling reaction with a good reaction yield [52], and **L2** was obtained through the methylation of **L1**. When the ligand was exchanged from one of the bipyridine ligands in *cis*-bis(bipyridyl)Ru(II) dichloride [53] to **L1**, deboronation proceeded, and **H-*n*CB-Ru** was obtained. In the case of **Me-*n*CB-Ru**, tetrabutylammonium fluoride (TBAF) was needed as a nucleophile for deboronation. Both compounds were characterized with ^{1}H, ^{13}C, and ^{11}B NMR spectroscopies and high-resolution mass measurements (see Supplementary Material, Charts S1–S20).

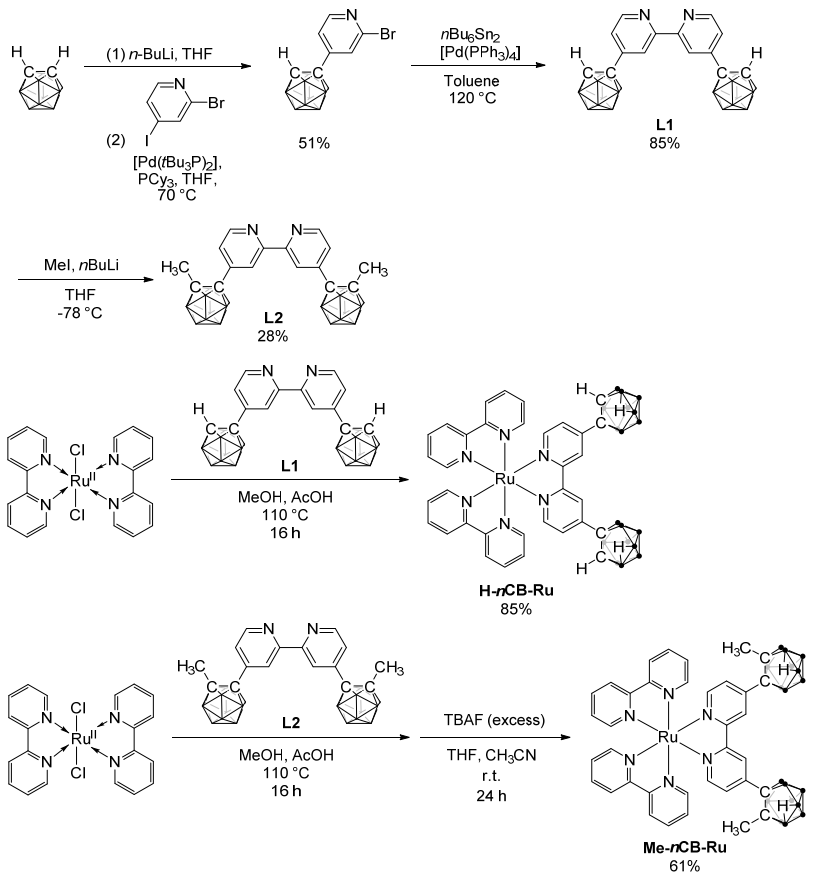

Scheme 1. Synthetic schemes of *nido*-carboranes.

2.2. Photophysical Properties o Ru(II) Complexes

Optical spectra are summarized in Figure 2 and the data are listed in Table 1. In the UV–vis absorption spectra in the EtOH/MeOH = 4/1 mixture solvent, the absorption bands were observed around 290 and 450 nm assigned to ligand-centered (LC) and metal-to-ligand

charge transfer (MLCT) transition, respectively (Figure 2a) [3]. In particular, redshifts of the MLCT absorption bands were detected from the *nido*-carborane-substituted complexes. In the photoluminescence (PL) spectra under argon for avoiding oxygen quenching, emission bands attributable to the phosphorescence of MLCT were obtained from all complexes (Figure 2b–d). In particular, **H-*n*CB-Ru** showed the band in the relatively longer wavelength region. These MLCT absorptions and emissions generally originated from the d–π^* transitions from the highest occupied molecular orbital (HOMO) localized in the metal center to the lowest unoccupied molecular orbital (LUMO) in the ligand [3]. Thus, the observed peak shifts indicate that strong electron donation from the anionic *nido*-carborane units should unstabilize HOMO followed by the narrow HOMO–LUMO energy gap. It should be mentioned that the red-shifted emission band was observed not from **Me-*n*CB-Ru** but from **H-*n*CB-Ru**, meaning that the substituent effect should significantly influence the electronic structure in the excited state. Similar to the results from *o*-carborane dyads, these data also represent that molecular conformations and rotations could play a critical role in the degree of electronic interaction between the Ru complex and *nido*-carborane units.

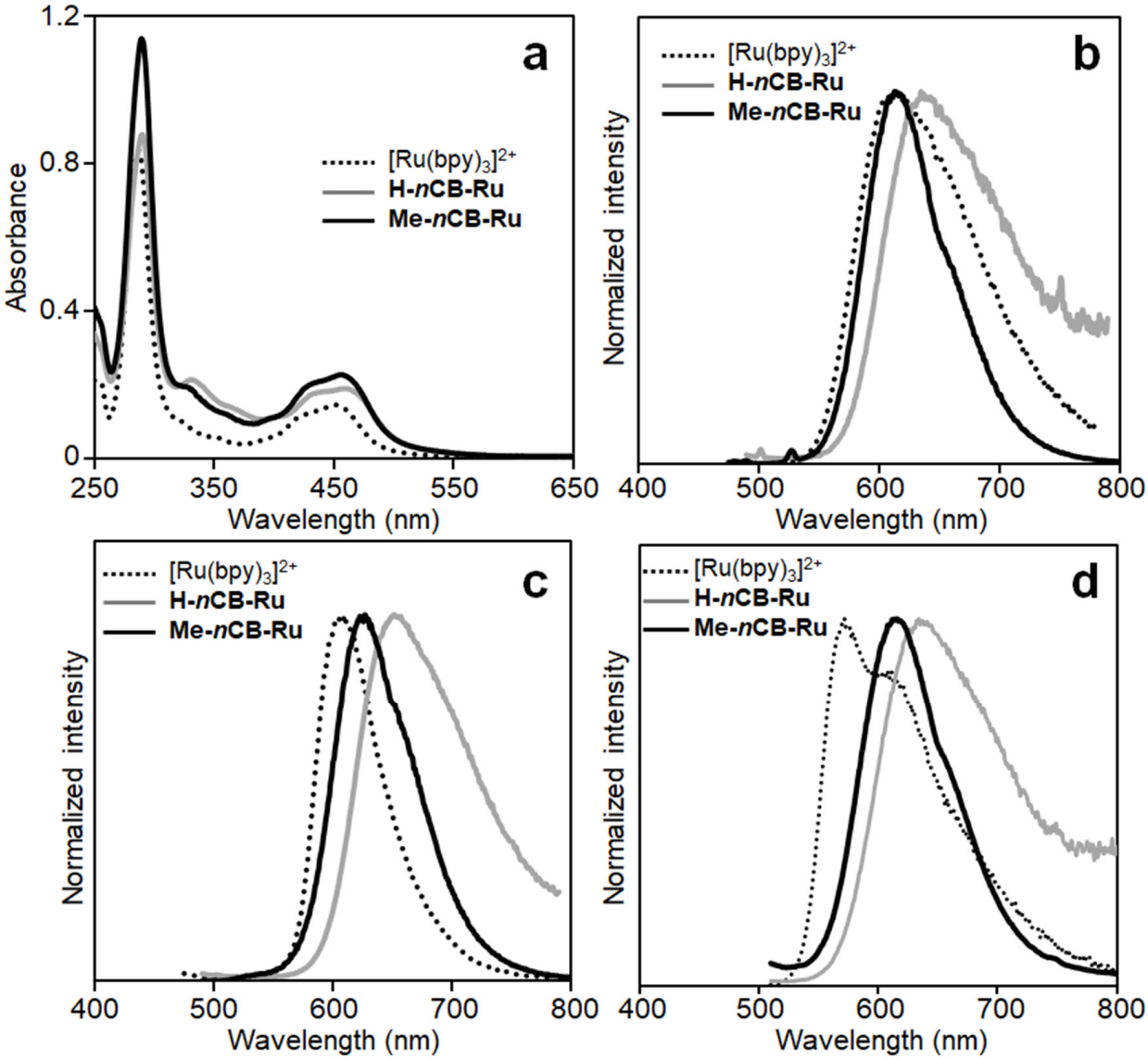

Figure 2. (**a**) UV–vis absorption and (**b**) phosphorescence spectra of the ruthenium complexes in EtOH/MeOH = 4/1 (1.0×10^{-5} M), (**c**) solid and (**d**) 1 wt% PEG films.

Table 1. Photophysical properties of the complexes [a].

Compound	ε [M^{-1} cm^{-1}]	λ_{ab} [nm]	λ_{em_RT} [nm] [b]	Φ_{RT} [c]	τ_{RT} [ns] [d]	k_r [10^6 s^{-1}]	k_{nr} [10^6 s^{-1}]	λ_{em_77K} [nm]	Φ_{77K}
$[Ru(bpy)_3]^{2+}$	84,000	450	615	0.09	430	0.28	2.0	578	0.33
H-*n*CB-Ru	88,000	458	637	0.10	420	0.29	2.1	596	0.25
Me-*n*CB-Ru	110,000	457	614	0.015	170 (54%) 42 (46%)	0.14	6.6	583	0.39

[a] In EtOH/MeOH = 4/1 (1.0×10^{-5} M). [b] Excited at λ_{ab}. [c] Determined with the integrated sphere method. [d] Excited at 375 nm.

In comparison with phosphorescence quantum yields at room temperature (Φ_{RT}), it was found that the value of **Me-*n*CB-Ru** was crucially smaller than those of the other two complexes. In order to quantitatively evaluate kinetics in the decay processes, lifetimes were determined, and the rate constants of radiative (k_r) and non-radiative decay processes (k_{nr}) were calculated. Accordingly, the short lifetime component with the level of several tens of nanoseconds was observed only from **Me-*n*CB-Ru**. Correspondingly, larger k_{nr} was obtained than those of other complexes, meanwhile, the phosphorescence quantum yields at 77 K were observed at a similar level. From these results, it is suggested that the methyl group should facilitate non-radiative decay through molecular motions in solution.

Table 2 shows the photophysical properties in solid and in the PEG film containing 1 wt% each complex. In the solid states, significant bathochromic shifts and decreases in the phosphorescence quantum yields by the substitution of *nido*-carboranes were observed. Additionally, in comparison with the photophysical data in the solution states, $[Ru(bpy)_3]^{2+}$ exhibited almost the same optical properties, while **H-*n*CB-Ru** and **Me-*n*CB-Ru** showed differences in the optical data between solution and solid states. Therefore, in the case of $[Ru(bpy)_3]^{2+}$, it was suggested that there were slight intermolecular interactions to affect the optical properties in the solid-state. Conversely, in the solid states of **H-*n*CB-Ru** and **Me-*n*CB-Ru**, strong intermolecular interaction existed probably due to the large dipole moments between anionic *nido*-carborane units and the cationic ruthenium center, and the interaction caused the bathochromic shifts and the decreases in the phosphorescence quantum yields. In the PEG film, remarkable improvements in the phosphorescence quantum yields were exhibited by the introduction of *nido*-carboranes (Φ_{RT} = 0.03 → **H-*n*CB-Ru**: 0.14, **Me-*n*CB-Ru**: 0.11). According to kinetic information, these emission enhancements should be attributable to both increases in k_r and decreases in k_{nr}. Since the *nido*-carborane units improve the transition dipole moment by expanding the conjugation system, the electronic transition for emission should be accelerated. Therefore, larger k_r than that of the pristine complex is obtained. Further, it is likely that rigid and bulky *nido*-carborane units suppress intermolecular interactions as well as molecular motions in the condensed states. Thus, non-radiative decay should be disturbed.

Table 2. Photophysical properties of the complexes in solid state and 1 wt% PEG film.

	Solid					PEG				
Compound	λ_{em} [nm] [a]	Φ [b]	τ [ns] [c]	k_r [10^6 s^{-1}]	k_{nr} [10^6 s^{-1}]	λ_{em} [nm] [a]	Φ [b]	τ [ns] [c]	k_r [10^6 s^{-1}]	k_{nr} [10^6 s^{-1}]
$[Ru(bpy)_3]^{2+}$	607	0.08	340	0.24	2.7	572	0.03	270	0.11	3.7
H-*n*CB-Ru	651	0.04	190	0.21	5.1	634	0.14	670	0.19	1.2
Me-*n*CB-Ru	627	0.02	170	0.12	5.7	616	0.11	490	0.22	1.8

[a] Excited at λ_{ab} in EtOH/MeOH = 4/1 (1.0×10^{-5} M). [b] Determined with the integrated sphere method. [c] Excited at 375 nm.

2.3. Electrochemical Properties of Ru(II) Complexes

The electrochemical properties of each complex were examined by cyclic voltammetry (CV) in CH_3CN with 0.1 M Bu_4NPF_6 as a supporting electrolyte (Table 3 and Figure S1) [54]. Due to the narrow electrochemical windows of EtOH and MeOH, which were used in optical measurements as a solvent, we performed CV in CH_3CN. $[Ru(bpy)_3]^{2+}$, **H-*n*CB-Ru**, and **Me-*n*CB-Ru** displayed reduction peaks at −1.67, −1.70, and −1.68 V, respectively.

From peak onset potentials in cyclic voltammograms, LUMO energy levels were estimated, and subsequently, HOMO energy levels were calculated from the band gap energies estimated from the absorption edges (Figure 3). Comparing the frontier orbitals of the *nido*-carborane-substituted complexes with that of $[Ru(bpy)_3]^{2+}$, we found that the LUMO levels were slightly unstabilized, while the HOMO levels were significantly elevated. This result indicates that the electron-donating properties of the *nido*-carborane units only affected the HOMO levels of the complexes. In $[Ru(bpy)_3]^{2+}$ and its derivatives, it is supposed that HOMO is delocalized between the ruthenium center and the *nido*-carborane units, meanwhile, the LUMO is localized in bipyridine ligands. Therefore, only HOMO should be elevated by the substituent effect at the ligand units. Hence, the emission band should be obtained in the longer wavelength region. These transitions were called mixed metal–ligand-to-ligand charge transfer (MLLCT) [9].

Table 3. Electrochemical properties for the ruthenium complexes.

Compound	$E_{red,onset}$ [V] [a]	$E_{LUMO,CV}$ [V] [b]	$E_{HOMO,opt}$ [eV] [c]	$E_{g,opt}$ [eV] [d]
$[Ru(bpy)_3]^{2+}$	−1.67	−3.43	−5.97	2.54
H-*n*CB-Ru	−1.70	−3.40	−5.86	2.46
Me-*n*CB-Ru	−1.68	−3.42	−5.90	2.48

[a] Onset potential of first reduction wave. [b] Calculated from the empirical formula, LUMO = $-E_{red,onset} - 5.10$ (eV). [c] HOMO = LUMO − $E_{g,opt}$ (eV). [d] Band gap energy: $E_g = 1240/\lambda_{ab,edge}$.

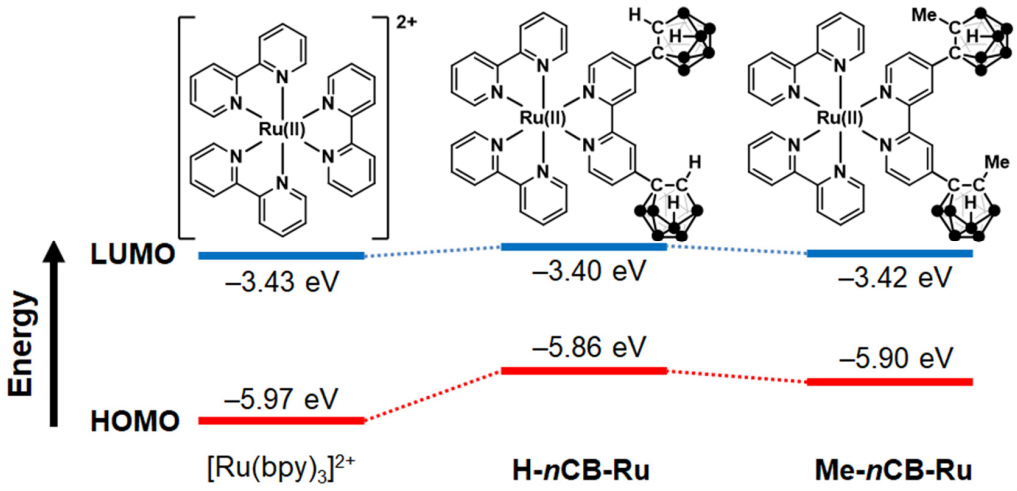

Figure 3. Estimated energy levels of frontier orbitals of the ruthenium complexes from electrochemical and optical data.

2.4. DFT Calculations

The optimized geometries of each complex in the ground (S_0) and lowest-lying triplet excited (T_1) states were estimated using unrestricted B3LYP with the 6-31G(d) basis set for all atoms except for the ruthenium atom which was treated with LANL2DZ effective core potentials (ECPs) and corresponding basis sets [55]. Vertical excitation energies were calculated using time-dependent DFT (TD-DFT) with the same set of functionals and basis sets. In order to include the solvation effect of CH_3CN, the polarizable continuum model (PCM) was used in these calculations. All calculations were performed using the GAUSSIAN 16 program. Table 4 shows the absorption data calculated at the optimized S_0 geometries of each complex. In order to obtain a qualitative description of the electronic transitions which represent absorption behaviors, the analysis with natural transition orbitals (NTOs), which was generated from the complicated ordinary orbital representation as single or double pairs of orbitals for each transition, was carried out [56]. The optimized

S_0 geometries of each complex and their highest occupied transition orbitals (HOTOs) and lowest unoccupied transition orbitals (LUTOs) for the main allowed transitions are illustrated in Figure 4. Corresponding results to experimental data as shown in Table 1 were obtained from calculations. In $[Ru(bpy)_3]^{2+}$ and **Me-*n*CB-Ru**, their NTOs show similar features in that the HOTOs are localized in the d-orbitals of ruthenium, whereas the LUTOs are localized in the π*-orbitals of bipyridine ligands. Note that there is no contribution of the *nido*-carborane units to HOTO and/or LUTO in **Me-*n*CB-Ru**, meanwhile, in the case of **H-*n*CB-Ru**, the LUTO is localized in the bipyridine moiety and the HOTO is delocalized in the *nido*-carborane units as well as ruthenium. According to these results and the electrochemical data (Table 3), MLLCT is certainly the major absorption transition in **H-*n*CB-Ru**. These behaviors correspond to the experimental data.

Table 4. Estimated absorption data from TD-DFT calculations.

Compound	$\lambda_{ab,calc}$ [nm]	$E_{g,calc}$ [eV]	*f*	Transitions [a]
$[Ru(bpy)_3]^{2+}$	408	3.04	0.1254	H − 2 → L (17%), H − 2 → L + 1 (35%), H − 2 → L + 2 (3%), H − 1 → L (4%), H − 1 → L + 1 (3%), H − 1 → L + 2 (33%)
H-*n*CB-Ru	425	2.92	0.2424	H − 5 → L + 2 (6%), H − 3 → L + 1 (23%), H − 2 → L + 1 (6%), H → L + 2 (60%)
Me-*n*CB-Ru	407	3.05	0.1662	H − 4 → L + 1 (52%), H − 3 → L (10%), H − 3 → L + 2 (33%)

[a] H = HOMO and L = LUMO.

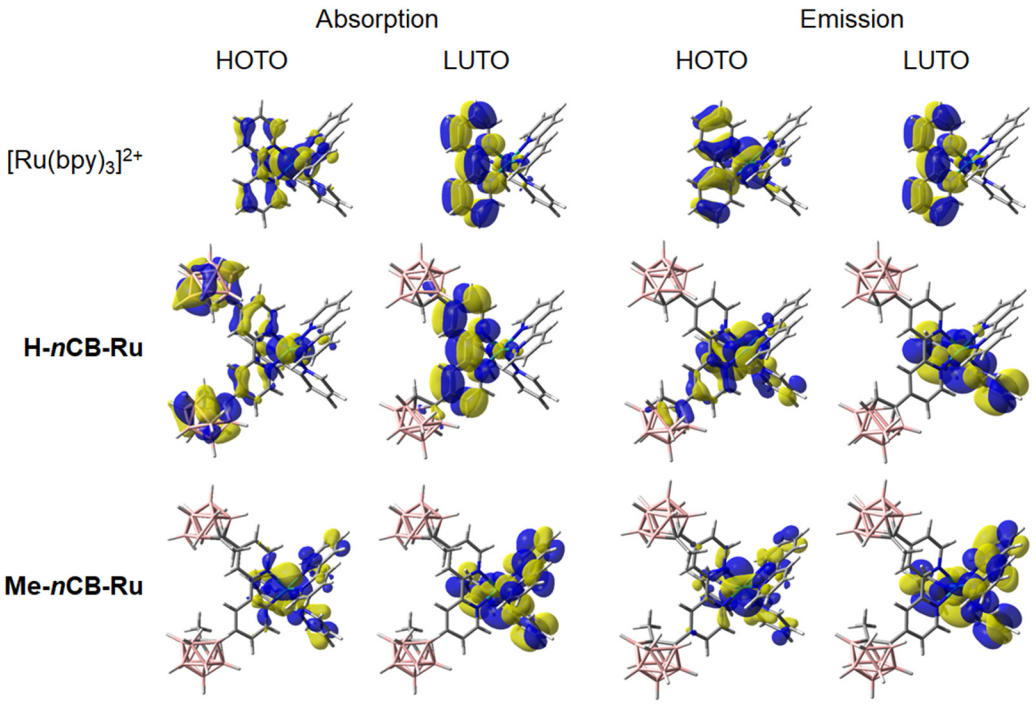

Figure 4. Natural transition orbitals calculated from the transitions of absorption and emission with the ruthenium complexes.

To gather deep insight regarding the substituent effect on the contributions of the *nido*-carborane units to NTOs between **H-*n*CB-Ru** and **Me-*n*CB-Ru**, the dihedral angles (φ_H and φ_{Me}, respectively), between the C–C bond in *nido*-carborane and the π-plane of the bipyridine ligand were evaluated in the optimized S_0 geometries. Significantly, the φ_H and φ_{Me} angles are 13.9° (parallel state) and 71.2° (twisted state), respectively (Figure 1),

indicating that the substituent should play a critical role in the determination of molecular conformations where the bipyridine moiety is roughly co-planar or orthogonal to the five-membered ring of *nido*-carborane. Moreover, energy level diagrams upon rotation of the *nido*-carborane units were obtained by relaxed scanning (Figure 5). The calculated rotational barriers of **H-*n*CB-Ru** and **Me-*n*CB-Ru** are 0.10 and 0.18 eV, respectively, suggesting that **H-*n*CB-Ru** prefers to form the parallel distribution for the extension of the conjugation system and resonant electron-donating of the *nido*-carborane unit, while **Me-*n*CB-Ru** was forced to be in the twisted state because of the steric hindrance between the bulky methyl group and bipyridine moiety. In summary, it is revealed that the dihedral angle between π-plane of bipyridine and *nido*-carborane is largely determined by the substituent effect. In the parallel and twisted conformation, the degree of electronic donation from the *nido*-carborane unit is intrinsically changed (parallel: strong, twist: weak). Based on this *angle-dependent electron-donating effect*, the electronic properties of the ruthenium complex are varied.

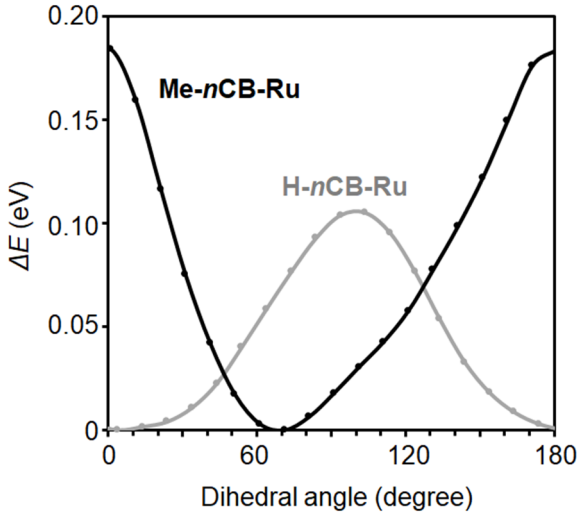

Figure 5. Energy level diagrams of the S_0 state for each complex upon rotation of the *nido*-carborane units.

Table 5 shows the emission data calculated with the TD-DFT method at the optimized T_1 geometries. Further, NTO analyses were performed at the geometries. The optimized T_1 geometries of each complex and their HOTOs and LUTOs are illustrated in Figure 4. The features of the NTOs for each emission transition were almost the same as that of absorption. Additionally, the dipole moments in the ground and excited states (MLCT states) of each complex were calculated (Table 6). It was shown that *nido*-carborane-substituted ruthenium complexes have significantly large dipole moments in comparison to $[Ru(bpy)_3]^{2+}$ derived from the anionic *nido*-carborane units and the cationic ruthenium center. In the case of **H-*n*CB-Ru** and **Me-*n*CB-Ru**, the dipole moments in the MLCT states are smaller than those of ground states because the directions of MLCT are opposite to the vectors of original dipole moments. In particular, the dipole moments of **H-*n*CB-Ru** are smaller than those of **Me-*n*CB-Ru,** especially in the MLCT state. From these data, it is proposed that the delocalization of negative charge on the *nido*-carborane units could occur by the formation of the MLLCT state in **H-*n*CB-Ru**. In contrast, the electron density on the *nido*-carborane units should be larger because **Me-*n*CB-Ru** forms the MLCT state. In other words, negative charges are dispersed in the whole **H-*n*CB-Ru** molecule, whereas the negative charge should be localized at the ruthenium complex moiety in the excited state of **Me-*n*CB-Ru**. The delocalized charge would weaken to make electronic interactions to polar solvents in the charge-separated excited state. As a result, relatively larger Φ_{RT} can be obtained from **H-*n*CB-Ru** than that from **Me-*n*CB-Ru** through the suppression of non-radiative decay caused by non-specific interaction with solvents.

Table 5. Calculated emission data from TD-DFT at the optimized T_1 geometries.

Compound	$\lambda_{em,calc}$ [nm]	$E_{g,calc}$ [eV]	Transitions [a]
$[Ru(bpy)_3]^{2+}$	620	2.00	H − 3 → L (6%), H → L (86%), H → L + 1 (2%)
H-*n*CB-Ru	649	1.91	H − 6 → L (3%), H − 2 → L (44%), H → L (42%)
Me-*n*CB-Ru	562	2.21	H − 8 → L (2%), H − 2 → L + 1 (86%), H → L + 1 (4%)

[a] H = HOMO and L = LUMO.

Table 6. Calculated dipole moments at the optimized structures.

Compound	μ_{ground} [Debye]	μ_{MLCT} [Debye]	$\Delta\mu$ [Debye]
$[Ru(bpy)_3]^{2+}$	0.01	7.37	+7.4
H-*n*CB-Ru	63.4	56.9	−6.5
Me-*n*CB-Ru	66.9	61.2	−5.7

3. Conclusions

nido-Carborane-substituted tris(2,2′-bipyridyl)ruthenium(II) complexes, **H-*n*CB-Ru** and **Me-*n*CB-Ru**, were synthesized. We initially show that *nido*-carborane should be an effective electron donor because of deep-red phosphorescence with good phosphorescent quantum yields from the PEG films containing the complexes. Furthermore, from the experimental and computational studies, it was shown that the electron-donating properties of the *nido*-carborane units and the optical properties were tunable by controlling the dihedral angles between bipyridine moieties and five-membered ring planes with steric substituents. It should be emphasized that this is the first study to demonstrate the angle-dependent variable contributions of the *nido*-carborane units to the electronic and optical properties of phosphorescent compounds. In other words, another unique electronic character can be found originating from the 3D aromaticity property of the boron clusters.

Supplementary Materials: The following supporting information can be downloaded at: https://www.mdpi.com/article/10.3390/cryst12050688/s1, Charts S1–S15: NMR spectra; Charts S16–S20: mass spectra; Figure S1: Cyclic voltammograms for Ru complexes in CH_3CN with 0.1 M Bu_4NPF_6 at 50 mV s^{-1}. The horizontal scale refers to an Fc/Fc^+ electrode.

Author Contributions: Data curation, K.U.; Formal analysis, K.U.; Funding acquisition, K.T.; Project administration, K.T. and Y.C.; Supervision, Y.C.; Writing—original draft, K.U. and K.T.; Writing—review & editing, K.T. All authors have read and agreed to the published version of the manuscript.

Funding: This work was partially supported by the Nakatani Foundation (for Kazuo Tanaka) and JSPS KAKENHI Grant Numbers JP21H02001 and JP21K19002 (for Kazuo Tanaka).

Institutional Review Board Statement: Not applicable.

Informed Consent Statement: Not applicable.

Data Availability Statement: The data presented in this study are available on request from the corresponding author.

Conflicts of Interest: The authors declare no conflict of interest.

References

1. Juris, A.; Balzani, V.; Barigelletti, F.; Campagna, S.; Belser, P.; von Zelewsky, A. Absorption and electrochemical properties of ruthenium(II) dyes, studied by semiempirical quantum chemical calculations. *Coord. Chem. Rev.* **1988**, *84*, 85–277.
2. Young, R.C.; Meyer, T.J.; Whitten, D.G. Kinetic relaxation measurement of rapid electron transfer reactions by flash photolysis. Conversion of light energy into chemical energy using the tris(2,2′-bipyridine)ruthenium(3+)-tris(2,2′-bipyridine)ruthenium(2+*) couple. *J. Am. Chem. Soc.* **1975**, *97*, 4781–4782. [CrossRef]
3. Lytle, F.E.; Hercules, D.M. Luminescence of tris(2,2′-bipyridine)ruthenium(II) dichloride. *J. Am. Chem. Soc.* **1969**, *91*, 253–257. [CrossRef]

4. Baba, A.I.; Shaw, J.R.; Simon, J.A.; Thummel, R.P.; Schmehl, R.H. The photophysical behavior of d^6 complexes having nearly isoenergetic MLCT and ligand localized excited states. *Coord. Chem. Rev.* **1998**, *171*, 43–59. [CrossRef]
5. McClenaghan, N.D.; Leydet, Y.; Maubert, B.; Indelli, M.T.; Campagna, S. Excited-state equilibration: A process leading to long-lived metal-to-ligand charge transfer luminescence in supramolecular systems. *Coord. Chem. Rev.* **2005**, *249*, 1336–1350. [CrossRef]
6. Xia, H.; Zhang, C.; Liu, X.; Qiu, S.; Lu, P.; Shen, F.; Zhang, J.; Ma, Y. Ruthenium(II) Complex as Phosphorescent Dopant for Highly Efficient Red Polymers Light-Emitting Diodes. *J. Phys. Chem. B* **2004**, *108*, 3185–3190. [CrossRef]
7. Zhu, Y.; Gu, C.; Tang, S.; Fei, T.; Gu, X.; Wang, H.; Wang, Z.; Wang, F.; Lu, D.; Ma, Y. A new kind of peripheral carbazole substituted ruthenium(II) complexes for electrochemical deposition organic light-emitting diodes. *J. Mater. Chem.* **2009**, *19*, 3941–3949. [CrossRef]
8. Li, J.; Hai, Z.; Xiao, H.; Yi, X.; Liang, G. Intracellular self-assembly of $Ru(bpy)_3^{2+}$ nanoparticles enables persistent phosphorescence imaging of tumors. *Chem. Commun.* **2018**, *54*, 3460–3463. [CrossRef]
9. Charboneau, D.J.; Piro, N.A.; Kassel, W.S.; Dudley, T.J.; Paul, J.J. Structural, electronic and acid/base properties of $[Ru(bpy)(bpy(OH)_2)_2]^{2+}$ (bpy = 2,2′-bipyridine, $bpy(OH)_2$ = 4,4′-dihydroxy-2,2′-bipyridine). *Polyhedron* **2015**, *91*, 18–27. [CrossRef]
10. Poater, J.; Viñas, C.; Bennour, I.; Escayola, S.; Solà, M.; Teixidor, F. Too Persistent to Give Up: Aromaticity in Boron Clusters Survives Radical Structural Changes. *J. Am. Chem. Soc.* **2020**, *142*, 9396–9407. [CrossRef]
11. Poater, J.; Solà, M.; Viñas, C.; Teixidor, F. π-Aromaticity and Three-Dimensional Aromaticity: Two sides of the Same Coin? *Angew. Chem. Int. Ed.* **2014**, *53*, 12191–12195. [CrossRef] [PubMed]
12. Teixidor, F.; Núñez, R.; Viñas, C.; Sillanpää, R.; Kivekäs, R. The Distinct Effect of the *o*-Carboranyl Fragment: Its Influence on the I–I Distance in R_3PI_2 Complexes. *Angew. Chem. Int. Ed.* **2000**, *39*, 4290–4292. [CrossRef]
13. Núñez, R.; Farràs, P.; Teixidor, F.; Viñas, C.; Sillanpää, R.; Kivekäs, R. A Discrete PI–IP Assembly: The Large Influence of Weak Interactions on the ^{31}P NMR Spectra of Phosphane–Diiodine Complexes. *Angew. Chem. Int. Ed.* **2006**, *45*, 1270–1272. [CrossRef] [PubMed]
14. Lee, H.-S.; Bae, J.-Y.; Ko, J.; Kang, Y.S.; Kim, H.S.; Kim, S.-J.; Chung, J.-H.; Kang, S.O. New Group 9 metal complexes containing N,P-chelate ligand system. *J. Organomet. Chem.* **2000**, *614–615*, 48–56. [CrossRef]
15. Nishino, K.; Morisaki, Y.; Tanaka, K.; Chujo, Y. Electron-Donating Abilities and Luminescent Properties of Tolane-Substituted *nido*-Carboranes. *New J. Chem.* **2017**, *15*, 10550–10554. [CrossRef]
16. Teixidor, F.; Núñez, R.; Viñas, C.; Sillanpää, R.; Kivekäs, R. Contribution of the *nido*-[7,8-$C_2B_9H_{10}$]-Anion to the Chemical Stability, Basicity, and ^{31}P NMR Chemical Shift in *nido*-*o*-Carboranylmonophosphines. *Inorg. Chem.* **2001**, *40*, 2587–2594. [CrossRef] [PubMed]
17. Valliant, J.; Guenther, K.; King, A.; Morel, P.; Schaffer, P.; Sogbein, O.; Stephenson, K. The medicinal chemistry of carboranes. *Coord. Chem. Rev.* **2002**, *232*, 173–230. [CrossRef]
18. Hawthorne, M.F.; Young, D.C.; Andrews, T.D.; Howe, D.V.; Pilling, R.L.; Pitts, A.D.; Reintjes, M.; Warren, L.F.; Wegner, P.A. π-Dicarbollyl derivatives of the transition metals. Metallocene analogs. *J. Am. Chem. Soc.* **1968**, *90*, 879–896. [CrossRef]
19. Safronov, A.V.; Shlyakhtina, N.I.; Everett, T.A.; VanGordon, M.R.; Sevryugina, Y.V.; Jalisatgi, S.S.; Hawthorne, M.F. Direct Observation of Bis(dicarbollyl)nickel Conformers in Solution by Fluorescence Spectroscopy: An Approach to Redox-Controlled Metallacarborane Molecular Motors. *Inorg. Chem.* **2014**, *53*, 10045–10053. [CrossRef]
20. Axtell, J.C.; Kirlikovali, K.O.; Djurovich, P.I.; Jung, D.; Nguyen, V.T.; Munekiyo, B.; Royappa, A.T.; Rheingold, A.L.; Spokoyny, A.M. Blue Phosphorescent Zwitterionic Iridium(III) Complexes Featuring Weakly Coordinating *nido*-Carborane-Based Ligands. *J. Am. Chem. Soc.* **2016**, *138*, 15758–15765. [CrossRef]
21. Visbal, R.; Ospino, I.; López-de-Luzuriaga, J.M.; Laguna, A.; Gimeno, M.C. N-Heterocyclic Carbene Ligands as Modulators of Luminescence in Three-Coordinate Gold(I) Complexes with Spectacular Quantum Yields. *J. Am. Chem. Soc.* **2013**, *135*, 4712–4715. [CrossRef] [PubMed]
22. Shi, C.; Sun, H.; Jiang, Q.; Zhao, Q.; Wang, J.; Huang, W.; Yan, H. Carborane tuning of photophysical properties of phosphorescent iridium(iii) complexes. *Chem. Commun.* **2013**, *49*, 4746–4748. [CrossRef] [PubMed]
23. Popescu, A.R.; Teixidor, F.; Viñas, C. Metal promoted charge and hapticities of phosphines: The uniqueness of carboranylphosphines. *Coord. Chem. Rev.* **2014**, *269*, 54–84. [CrossRef]
24. Sivaev, I.B.; Stogniy, M.Y.; Bregadze, V.I. Transition metal complexes with carboranylphosphine ligands. *Coord. Chem. Rev.* **2021**, *436*, 213795–213889. [CrossRef]
25. Kim, T.; Kim, H.; Lee, K.M.; Lee, Y.S.; Lee, M.H. Phosphorescence Color Tuning of Cyclometalated Iridium Complexes by *o*-Carborane Substitution. *Inorg. Chem.* **2013**, *52*, 160–168. [CrossRef] [PubMed]
26. Wang, H.; Wang, Y.; Li, H.-W.; Xie, Z. Synthesis, Structural Characterization, and Olefin Polymerization Behavior of Group 4 Metal Complexes with Constrained-Geometry Carborane Ligands. *Organometallics* **2001**, *20*, 5110–5118. [CrossRef]
27. Chujo, Y.; Tanaka, K. New Polymeric Materials Based on Element-Blocks. *Bull. Chem. Soc. Jpn.* **2015**, *88*, 633–643. [CrossRef]
28. Gon, M.; Tanaka, K.; Chujo, Y. Recent Progress in the Development of Advanced Element-Block Materials. *Polym. J.* **2018**, *50*, 109–126. [CrossRef]
29. Gon, M.; Tanaka, K.; Chujo, Y. Concept of Excitation-Driven Boron Complexes and Their Applications for Functional Luminescent Materials. *Bull. Chem. Soc. Jpn.* **2019**, *92*, 7–18. [CrossRef]

30. Ito, S.; Gon, M.; Tanaka, K.; Chujo, Y. Molecular Design and Applications of Luminescent Materials Composed of Group 13 Elements with an Aggregation-Induced Emission Property. *Natl. Sci. Rev.* **2021**, *8*, nwab049. [CrossRef]
31. Ochi, J.; Tanaka, K.; Chujo, Y. Recent Progresses in the Development of Solid-state Luminescent *o*-Carboranes with Stimuli Responsivity. *Angew. Chem. Int. Ed.* **2020**, *132*, 9841–9855. [CrossRef] [PubMed]
32. Ochi, J.; Tanaka, K.; Chujo, Y. Experimental Proofs for Emission Annihilation through Bond Elongation at the Carbon–Carbon Bond in *o*-Carborane with Fused Biphenyl-Substituted Compounds. *Dalton Trans.* **2021**, *50*, 1025–1033. [CrossRef] [PubMed]
33. Naito, H.; Nishino, K.; Morisaki, Y.; Tanaka, K.; Chujo, Y. Solid-State Emission of the Anthracene–o-Carborane Dyad via Twisted-Intramolecular Charge Transfer in the Crystalline State. *Angew. Chem. Int. Ed.* **2017**, *56*, 254–259. [CrossRef] [PubMed]
34. Nishino, K.; Yamamoto, H.; Tanaka, K.; Chujo, Y. Solid-State Themochromic Luminescence via Twisted Intramolecular Charge Transfer and Excimer Formation of the Carborane-Pyrene Dyad with an Ethynyl Spacer. *Asian J. Org. Chem.* **2017**, *6*, 1818–1822. [CrossRef]
35. Nishino, K.; Uemura, K.; Tanaka, K.; Chujo, Y. Dual Emission via Remote Control of Molecular Rotation of *o*-Carborane in the Excited State by the Distant Substituents in Tolane-Modified Dyads. *New J. Chem.* **2018**, *16*, 4210–4214. [CrossRef]
36. Ochi, J.; Yuhara, K.; Tanaka, K.; Chujo, Y. Controlling the Dual-Emission Character of Aryl-Modified *o*-Carboranes by Intramolecular CH···O Interaction Sites. *Chem. Eur. J.* **2022**, *28*, e202200155. [CrossRef]
37. Nishino, K.; Tanaka, K.; Chujo, Y. Tuning of Sensitivity in Thermochromic Luminescence by Regulating Molecular Rotation Based on Triphenylamine-Substituted *o*-Carboranes. *Asian J. Org. Chem.* **2019**, *8*, 2228–2232. [CrossRef]
38. Naito, H.; Uemura, K.; Morisaki, Y.; Tanaka, K.; Chujo, Y. Enhancement of Luminescence Efficiencies by Thermal Rearrangement from *ortho*- to *meta*-Carborane in Bis-Carborane-Substituted Acenes. *Eur. J. Org. Chem.* **2018**, *2018*, 1885–1890. [CrossRef]
39. Naito, H.; Nishino, K.; Morisaki, Y.; Tanaka, K.; Chujo, Y. Highly-Efficient Solid-State Emissions of the Anthracene–*o*-Carborane Dyads with Various Substituents and Their Thermochromic Luminescent Properties. *J. Mater. Chem. C* **2017**, *4*, 10047–10054. [CrossRef]
40. Naito, H.; Nishino, K.; Morisaki, Y.; Tanaka, K.; Chujo, Y. Luminescence Color tuning of Stable Luminescent Solid Materials from Blue to NIR Based on Bis-*o*-Carborane-Substituted Oligoacenes. *Chem. Asian J.* **2017**, *12*, 2134–2138. [CrossRef]
41. Nishino, K.; Yamamoto, H.; Tanaka, K.; Chujo, Y. Development of Solid-State Emissive Materials Based on Multi-Functional *o*-Carborane-Pyrene Dyads. *Org. Lett.* **2016**, *18*, 4064–4067. [CrossRef] [PubMed]
42. Yuhara, K.; Tanaka, K.; Chujo, Y. Regulation of Solid-state Dual-emission Properties by Switching Luminescent Processes Based on the Bis-*o*-carborane-modified Anthracene Triad. *Mater. Chem. Front.* **2022**. [CrossRef]
43. Yamamoto, H.; Ochi, J.; Yuhara, K.; Tanaka, K.; Chujo, Y. Switching between Intramolecular Charge Transfer and Excimer Emissions in Solids Based on Aryl-modified Ethynyl–*o*-Carboranes. *Cell Rep. Phys. Sci.* **2022**, *3*, 100758. [CrossRef]
44. Wada, K.; Hashimoto, K.; Ochi, J.; Tanaka, K.; Chujo, Y. Rational Design for Thermochromic Luminescence in Amorphous Polystyrene Films with the Bis-*o*-carborane-substituted Enhanced-Conjugated Molecule Having Aggregation-Induced Luminochromism. *Aggregate* **2021**, *2*, e93.
45. Ochi, J.; Tanaka, K.; Chujo, Y. Dimerization-Induced Solid-State Excimer Emission Showing Consecutive Thermochromic Luminescence Based on Acridine-Modified *o*-Carboranes. *Inorg. Chem.* **2021**, *60*, 8990–8997. [CrossRef]
46. Nishino, K.; Yamamoto, H.; Tanaka, K.; Chujo, Y. Time-Dependent Emission Enhancement of the Etynylpyrene-o-Carborane Dyad and Its Application as a Luminescent Color Sensor for Evaluating Water Contents in Organic Solvents. *Chem. Asian J.* **2019**, *14*, 1577–1581. [CrossRef]
47. Ochi, J.; Tanaka, K.; Chujo, Y. Improvement of Solid-State Excimer Emission of the Aryl–Ethynyl–*o*-Carborane Skeleton by Acridine Introduction. *Eur. J. Org. Chem.* **2019**, *2019*, 2984–2988. [CrossRef]
48. Nishino, K.; Tanaka, K.; Morisaki, Y.; Chujo, Y. Design of Thermochromic Luminescence without Conformation and Morphology Changes by Employing the Bis(*o*-carborane)-Substituted Benzobithiophene Structure. *Chem. Asian J.* **2019**, *14*, 789–795. [CrossRef]
49. Nishino, K.; Uemura, K.; Tanaka, K.; Morisaki, Y.; Chujo, Y. Modulation of the *cis*- and *trans*-Conformations in the Bis-*o*-carborane Substituted Benzodithiophenes and Emission Enhancement Effect on Luminescent Efficiency by Solidification. *Eur. J. Org. Chem.* **2018**, *2018*, 1507–1512. [CrossRef]
50. Mori, H.; Nishino, K.; Wada, K.; Morisaki, Y.; Tanaka, K.; Chujo, Y. Modulation of Luminescent Chromic Behaviors and Environment-Responsive Intensity Changes by Substituents in Bis-*o*-carborane-Substituted Conjugated Molecules. *Mater. Chem. Front.* **2018**, *2*, 573–579. [CrossRef]
51. Nishino, K.; Hashimoto, K.; Tanaka, K.; Morisaki, Y.; Chujo, Y. Comparison of Luminescent Properties of Helicene-Like Bibenzothiophenes with *o*-Carborane and 5,6-Dicarba-*nido*-decaborane. *Sci. China Chem.* **2018**, *61*, 940–946. [CrossRef]
52. Li, X.; Tong, X.; Yin, Y.; Yan, H.; Lu, C.; Huang, W.; Zhao, Q. Using highly emissive and environmentally sensitive *o*-carborane-functionalized metallophosphors to monitor mitochondrial polarity. *Chem. Sci.* **2017**, *8*, 5930–5940. [CrossRef] [PubMed]
53. Sullivan, B.P.; Salmon, D.J.; Meyer, T.J. Mixed phosphine 2,2′-bipyridine complexes of ruthenium. *Inorg. Chem.* **1978**, *17*, 3334–3341. [CrossRef]
54. Sun, Y.; Hudson, Z.M.; Rao, Y.; Wang, S. Tuning and Switching MLCT Phosphorescence of $[Ru(bpy)_3]^{2+}$ Complexes with Triarylboranes and Anions. *Inorg. Chem.* **2011**, *50*, 3373–3378. [CrossRef] [PubMed]
55. Bae, H.J.; Chung, J.; Kim, H.; Park, J.; Lee, K.M.; Koh, T.-W.; Lee, Y.S.; Yoo, S.; Do, Y.; Lee, M.H. Deep Red Phosphorescence of Cyclometalated Iridium Complexes by o-Carborane Substitution. *Inorg. Chem.* **2014**, *53*, 128–138. [CrossRef]
56. Martin, R.L. Natural transition orbitals. *J. Chem. Phys.* **2003**, *118*, 4775–4777. [CrossRef]